



Nanotech Master 2018

**IBM Almaden
650 Harry Rd San Jose CA 95120
United States**

Characterization of metal oxide thin films for volatile organic compound detection

From March 01 2018 to August 31 2018

Conducted by :

- **Antoine PISSIS antoine.pissis@grenoble-inp.org**

Under the supervision of :

- **Company supervisor : Andrea FASOLI andrea.fasoli@ibm.com**
- **Phelma Tutor : Thierry OUISSSE thierry.ouisse@grenoble-inp.fr**

**Ecole nationale
supérieure de physique,
électronique, matériaux**

Phelma

Bât. Grenoble INP - Minatec
3 Parvis Louis Néel - CS 50257
F-38016 Grenoble Cedex 01

Tél +33 (0)4 56 52 91 00
Fax +33 (0)4 56 52 91 03

<http://phelma.grenoble-inp.fr>

CONFIDENTIAL

Abstract

English version

The success of big data analysis pushes the acquisition of a constantly growing amount of information. The types of information are diverse, and new types of information are emerging. An interesting type of information is the smell fingerprint, which can be used in various fields such as environment monitoring and healthcare. IBM research - Almaden chose to invest in a new application of gas sensors called electronic nose. From the different existing gas sensors technologies, the MOS technology has been selected for the use of electronic nose for its high sensitivity. The development of the next MOS gas sensors relies on the choice of the metal oxide synthesis process and the primary materials used. The evaluation of different processes requires a robust characterization set up to quantify the performance of the sensors.

Italian version

Il successo del settore di analisi dei big data sta spingendo l'acquisizione di informazioni sempre più ad alto livello. Le informazioni sono sempre più diversificate ed inoltre nuove informazioni aggiuntive stanno emergendo giorno dopo giorno. Un settore molto interessante può essere quello dei "smell fingerprint" applicabile a vari segmenti di mercato come quello ambientale o della sanità. IBM research Almaden ha deciso di investire in un nuovo tipo di sensori olfattivi, chiamati e-nose. Fra tutte le differenti tipologie di sensori esistenti l'azienda ha deciso di specializzarsi sui MOS gas sensors vista la loro elevata sensibilità. Lo sviluppo delle prossime generazioni di MOS gas sensors starà nella scelta del processo di sintesi degli ossidi metallici e sulla materia prima. Il giudizio sui differenti processi richiede una robusta caratterizzazione per quantificare le performance dei sensori.

French version

Le succès de la big data encourage l'accumulation et l'analyse d'une quantité toujours plus grande d'informations. Les informations récupérées sont diversifiées et on s'intéresse de plus en plus à de nouveaux types d'informations. En particulier, l'empreinte odorante s'est avérée intéressante pour certaines applications comme par exemple dans le contrôle de la pollution environnementale et dans la santé. IBM research - Almaden a choisi d'investir dans un nouveau type de détecteur de gaz appelé nez électronique. Parmi les technologies existantes, les détecteurs utilisant les oxydes de métaux ont été sélectionnés pour leur grande sensibilité. Le développement de la prochaine génération de tels détecteurs repose le choix du procédé de synthèse de l'oxyde de métal et des matériaux primaires utilisés. La validation d'un procédé nécessite la mesure des performances des capteurs par un système de test fiable.

Summary

Abstract	1
Summary	2
Acknowledgement	3
Glossary	4
Introduction	5
I. Literature review	7
1. Working principle of MOS gas sensor	7
2. Gas sensor objectives	9
3. Typical gas sensor response	10
4. Optimization of the gas sensor response	12
II. Fabrication review	14
1. MOS gas sensor architecture	14
2. Electrodes fabrication	15
3. MOS layer deposition	17
4. Contact pads deposition	18
III. Sensor characterization and work organization	20
1. Work organization	20
2. Characterization set up	21
3. Gas Delivery System	22
4. Solvent replacement study and interpretation	26
5. Improvement of the characterization set up for next study	33
Conclusion	34
Appendix	35
Bibliography	37

Acknowledgement

Firstly, I would like to express my gratitude to my IBM supervisor Dr. Andrea Fasoli who knew to provide me the right objectives to achieve an instructive Master thesis. I am grateful for his confidence, motivation and availability.

Besides my supervisor, I would like to thanks Dr. Luisa Bozano who made this project possible.

My sincere thanks also goes to Dr. Kristelle Lioni, Linda Sundberg, Ronald Labby, Amy Bowers, Dr Tim Erdmann, Charles Rettner and Alex Fritz who provided me an opportunity to join their team, and gave me access to the laboratory and research facilities. I would not be able to conduct this thesis without their precious support.

Last but not least, I thank my fellow teammates Angelo Milone, Sharon Morgan, Bastien Delaly and Michael Zanon for their help and stimulating discussions and especially Lisa Thornquist for her precious help for the redaction of this report.

Glossary

- IBM : International Business Machines Corporation
- MOS : Metal Oxide Semiconductor
- ppm : part per million
- ppb : parts per billion
- VOC : Volatile Organic Compound
- S and S^* : sensitivity
- NMP : N-méthyl-2-pyrrolidone
- DICO : Delayed Ignition of Autocatalytic Combustion Precursors
- TMAH : Tetramethylammonium hydroxide
- HMDS : bis(triméthylsilyl)amine
- NMP : N-méthyl-2-pyrrolidone
- MFC : mass flow controllers
- PMOH : Propylene glycol methyl ether

Introduction

In the 1950's, International Business Machines Corporation (IBM) Research contributed to the birth of the Silicon Valley by setting its first West Coast Laboratory in San Jose. Built a bit later in the 1980's, and located in the Santa Teresa County Park, IBM Research - Almaden focused and led the research efforts on many microelectronic fields such as data storage technology, data mining algorithms and the ability to position individual atoms. Today IBM Almaden is developing nanomedicine, services science, atomic scale storage, food safety and image analytics. The work presented in this report has been realized within the cognitive nose team within the Nanoscale Fabrication department.



Figure 1 : IBM Research - Almaden building

The sense of smell is, with the sense of taste, a challenging human sense to reproduce. The sense of smell makes possible to detect danger by smelling smoke or identify the scents exhaling from a flower. These smells are linked to the presence of specific Volatile Organic Compounds (VOC) in the air. VOC correspond to any chemical compound containing carbon whose vapor pressure at room temperature is high enough to be found as gases in the environment. VOC can be simple such as Methane CH_4 or more complex such as Acetone $(CH_3)_2CO_{(g)}$. Researchers and companies have developed technologies enabling the detection of the presence of these compounds. These technologies include metal oxide semiconductor (MOS) [1], carbon polymer composite [13] or gold nanoparticles [14]. The detection of smells can be found in various domains such as environmental pollution monitoring, food control and health diagnostics. The concentration of VOC involved in these applications varies from hundreds of ppm to fractions of ppb. Depending on the applications, sensors with high sensitivity must be considered. MOS gases sensors are well known for their high sensitivity [2]. This is the reason why this work is about MOS gas sensors. This work is

focusing on the characterization of MOS gas sensors in order to determine the influence of the metal oxide fabrication processes on the sensitivity of the gas sensors.

The first part of this report presents the principle of a MOS gas sensor. Then, in the second part, the fabrication steps realized in the IBM-Almaden facilities are discussed. And finally, the third part focuses on the characterization of the sensors. In this last part the set up used for the characterization will be described precisely.

I. Literature Review

Gas sensors based on metal oxide began to be developed in the early 60's for the detection of inflammable gases [3]. The current trend of Internet of Things (IoT) devices push the development of portable solutions for gas sensing and in particular MOS gas sensor even further [1]. This first part will present the basics of the MOS gas sensor operating principle and will present the definition of sensitivity used in this work.

1. Working Principle Of MOS Gas Sensor

The MOS gas sensor is based on the change in resistivity of a metal oxide film layer in the presence of a volatile compound. Tin oxide SnO_2 is often considered to make this sensitive layer. Other materials such as Zinc oxide ZnO_2 or Indium oxide In_2O_3 can also be used. This metal oxide layer can be represented as shown in Figure 2 by a stack of metal oxide grains. To measure the change of resistivity, the metal oxide layer is deposited above two electrodes between which a constant voltage bias is applied. The change of resistivity is calculated from the variation of current.

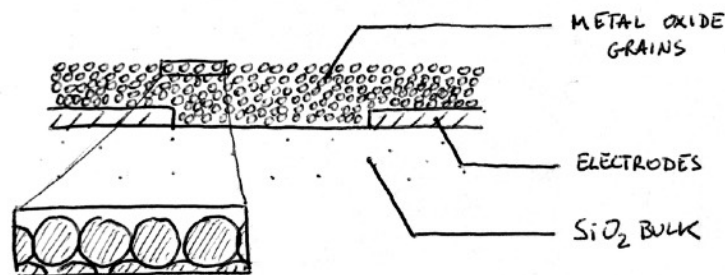


Figure 2 : Schematic of a thin film MOS gas sensor

The chemical mechanisms which lead to a change of resistivity of the metal oxide layer are presented as follows. In room conditions, oxygen molecules $\text{O}_{2(g)}$ of the air tend to react at the surface of the metal oxide grains. As studied by Yamazoe [7] the surface of SnO_2 can be populated by different oxygen species depending on the temperature of the surface. Table 1 presents the maximum temperatures at which different species can be found, also called desorption temperatures. Below these temperatures, these different species are present on the surface of the metal oxide grains.

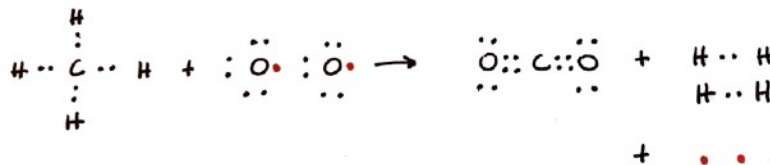
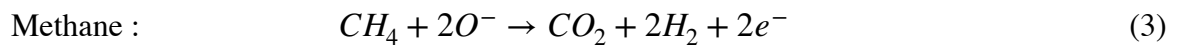
Gas	Desorption temperature	Species
O_2	80C	O_2
	150C	O_2^-
	520C	O^-
H_2O	110C	H_2O
	400C	$-OH$

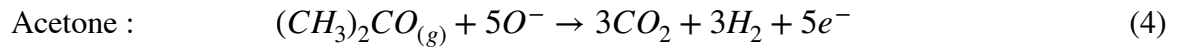
Table 1 : Desorption temperature for different oxygen species on SnO_2 surface

Considering the operating temperatures of the MOS gas sensors for this work are between 240 C and 400 C, and the desorption temperatures given in Table 1, the dominant species present at the metal oxide surface is O^- . At these temperatures oxygen binds to the surface by extracting an electron from the metal oxide according to equation (1).



This electron consumption creates a thin depleted skin around each metal oxide grain. For the electrons traveling inside the metal oxide by jumping from one grain to another, these depleted regions represent successive energy barriers. The thicker the depleted skin, the higher these energy barriers are and the higher the voltage applied must be for the electrons to move inside the metal oxide. As a consequence, the metal grain depletion due to the population of the oxygen species tends to increase the resistivity of the metal oxide. At 300C, VOC react with the oxygen species present at the surface of the metal, following equation (2) and competing with equation (1). Examples involving Methane $CH_{4(g)}$ and Acetone $(CH_3)_2CO_{(g)}$ are described by equation (3) and (4). These reactions are combustion type reactions and require high temperature to occur which is why the operating temperature of the sensors is 300C.





These reactions produce electrons which are injected back into the metal oxide. These combustion reactions lead to a new equilibrium state where the depleted skin of the metal oxide grain vanishes and the resistivity of the metal oxide decreases. Figure 3 shows the evolution of the metal oxide resistivity with the evolution of the depletion skin of the grains.

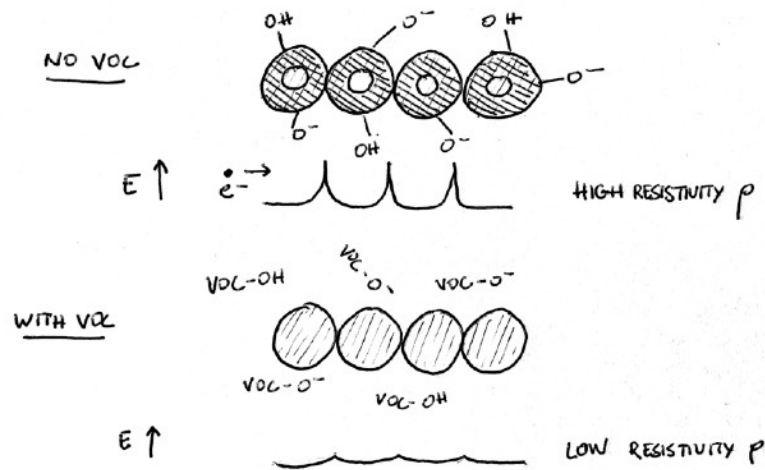


Figure 3 : The resistance of the metal oxide layer is given by the surface state of the metal oxide grains.

2. Gas Sensor Objectives

From understanding the working principle of a MOS gas sensor, the goal becomes to maximize its performances. Since this device is a sensor, its performances rest on its stability, sensitivity and selectivity. The definition of these three requirements and the reasons for their importance are presented in the following paragraphs.

A sensor is **stable** when its response is consistent over the time for identical perturbation. This is an important parameter if the sensor needs to be used multiple times over a long period. It has been observed that MOS gas sensors exhibit a slow decrease of resistance over time, resulting in a drifting global current. The reasons for this instability remain unclear but may be related to the change of morphology and properties of the metal oxide or the degradation of the electrodes as presented by Korotcenkov [10].

A sensor is **selective** when it reacts only for a specific perturbation - a particular volatile compound for the case of a gas sensor. Achieving perfect selectivity to any VOC appears difficult. Adding some dopants to the MOS layer has been shown to enhance the selectivity [11].

Instead of working on the selectivity of a single sensor, an other interesting solution is to combine the response of multiple sensors having significantly different response spectrum for different gases. This array of sensors also called e-nose is based on the model of the real human nose which is covered by a huge number and variety of bioreceptors [12].

The **sensitivity** of a sensor represents the capability of a sensor to detect the presence of a perturbation. The smaller is the perturbation detected the more sensitive is the sensor. A perturbation is detected when the variation the current induced is significantly higher than the amplitude of random fluctuations. In other words a minimum of signal and a minimum of signal to noise ratio are required both to maximize the sensitivity. The optimization of the sensitivity is the motivation of this work. The precise definition of the sensitivity used is presented in the next part.

3. Typical Gas Sensor Response

In order to determine the sensitivity of the sensor, the sensor must undergo a characterization test. The complete set up used for the characterization is presented in Part III. During a typical characterization run, the sensor received dry air during a period T_{init} then a small percentage of the target gas is introduced during a period $T_{exposure}$ and finally the sensor received dry again during a period $T_{recovery}$. A constant voltage bias V between the two electrodes of the device is applied, and the evolution of the current is measured. When the VOC is introduced, an increase of current is expected according to the chemical reduction reaction described in Part I.1. An example of a plot obtained is presented in Figure 4.

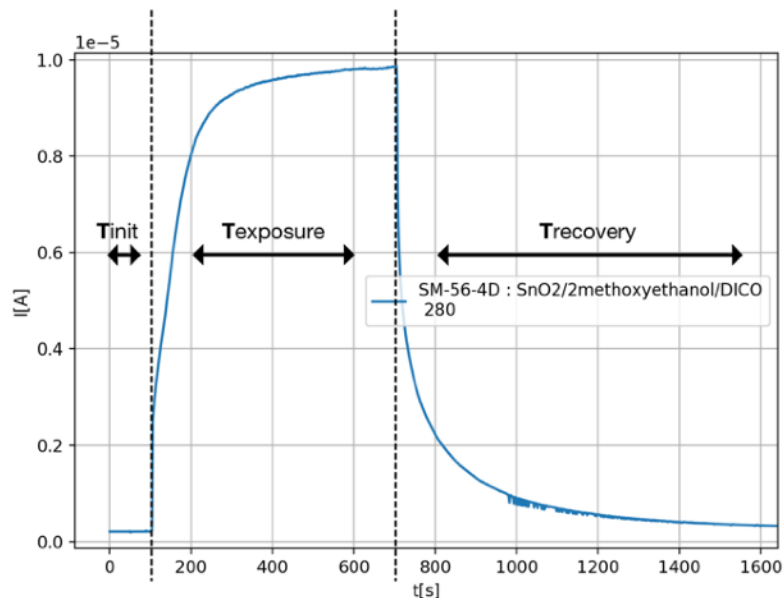


Figure 4 : Current response of a MOS gas sensor.

From the variation of the current between the three phases of the characterization test, different indicators can be extracted :

- **Baseline current** : stable current obtained when the analyte is not applied
- **Max current** : current obtained 500 sec after the introduction of the analyte
- **Delta current** : difference of current between baseline current and max current.

$$\Delta I = I_{max} - I_{baseline} \quad (5)$$

- **Sensitivity** : two different definitions of sensitivity are possible.

For these definition R_0 represents the initial resistance and R_{min} the resistance obtained when Max current is reached.

The first definition - more common - is defined from the ratio between the variation of resistance ΔR and the initial resistance R_0 :

$$S = \frac{\Delta R}{R_0} = \frac{R_0 - R_{min}}{R_0} = \frac{I_{max} - I_{baseline}}{I_{max}} = \frac{\Delta I}{I_{max}} \quad (6)$$

The second definition is given by the ratio between the initial resistance and the resistance obtained when Max current is reached :

$$S^* = \frac{R_0}{R_{min}} = \frac{I_{max}}{I_{baseline}} \quad (7)$$

These two definitions are equivalent since :

$$S = 1 - \frac{1}{S^*} \quad (8)$$

According to these expressions, the domain of definition are $S \in [0,1]$ for the first definition (6) and $S^* \in [1, +\infty[$ for the second definition (7). The domain of definition of S^* being wider than S , S^* appears to be a better definition to represent large variations in sensors resistances and to compare results of sensitivity from different sensor test runs. As a consequence, the definition of S^* (7) is mainly used in this report to represent the sensitivity.

- **Response time** : time necessary to reach 90% of the variation of current $\Delta I = I_{max} - I_{baseline}$ after the introduction of the analyte.
- **Recovery time** : time necessary to reach back 10% of the variation of current $\Delta I = I_{max} - I_{baseline}$ after removing the analyte.

The indicators presented are used to quantify and compare the different gas sensor current responses. It is possible then to identify the gas sensor which presents the best response performance.

4. Optimization Of The Gas Sensor Response

During the design of the gas sensor multiple parameters can be tuned in order to maximize its response performance.

- Some parameters for optimization are related to the architecture of the sensor. An important parameter is the **thickness of the metal oxide layer** which is deposited. It has been seen that relatively thin layers tend to present a faster response and a larger change of resistivity. This can be explained by the fact that VOC need to penetrate into the layer. For a thick layer only the surface responds as the active region and for a thin layer the entire layer is active as shown in Figure 5. A theoretical study involving VOC diffusion from Sakai [4] shows the relation between sensitivity and thickness of the layer. One result is the thinner the layer is, the more sensitive it is.

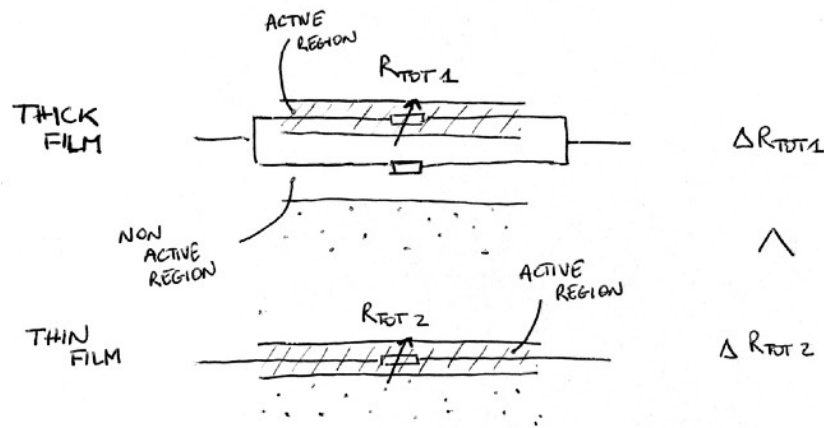


Figure 5 : Variation of resistance of a thick and a thin layer

- The conditions set for the operation of the gas sensor also influence its sensitivity.

The **working temperature** is an important parameter since it triggers the reaction between the VOC and the oxygen species present at the surface of the metal oxide grains. Results from Part III.4 show that there is an optimal working temperature for which the sensitivity is maximized. This peak of sensitivity can be visualized in the Sakai study [4]. This study also predicts that the optimal temperature increases when the thickness of the metal oxide layer decreases.

Another working condition which needs to be considered is the **voltage bias** which is applied between the two electrodes. The voltage applied needs to be relatively low to detect the fluctuation of the energy barriers at the grain boundaries, according to Varpula [5]. This is the reason the voltage applied during the characterization is in the order of 100 mV.

- The sensitivity depends on the **morphology of the metal oxide layer**. The metal oxide layer can have grains of different sizes and shapes. The layer may also vary in porosity. Indeed, depending on the fabrication process, pores can be observed at the surface of the metal oxide layer. By increasing the reactive surface area, pores increase the sensitivity and the reactivity of the sensor.

All of these previous parameters must be considered to improve the response performances of the sensor. In addition to that, these parameters can be correlated together. For example Korotcentkov [6] shows that, depending on the deposition technique, targeting different film thicknesses can result in different morphologies. In this study, thicker metal oxide films present larger grains. As a consequence it is difficult to tune each parameter separately.

Part II presents the global process flow of the MOS gas sensor fabrication. In Part III, an optimization of the sensor fabrication is presented.

II. Fabrication Review

Fabricating a MOS gas sensor involves multiple fabrication processes from microelectronics. In this second part, the global architecture of the MOS gas sensor used is described and divided into multiple elements. The process flows for the fabrication of each element are then presented. All the fabrication steps presented in this report were conducted at IBM Almaden.

1. MOS Gas Sensor Architecture

The schematic of the design of the MOS gas sensor alongside with one sensor obtained after fabrication is shown in Figure 6.



Figure 6 : Schematic of a MOS gas sensor and real sensors obtained after fabrication

On the MOS gas sensor schematic, three different elements can be identified - the electrodes, the active metal oxide layer and the contact pads. The substrate used is a silicon wafer with a 1 μm layer of silicon oxide SiO_2 on top in order to have a non-conductive surface. The electrodes are two metallic paths drawn directly on the SiO_2 surface used to apply the voltage bias and measure the current. The metal oxide layer is deposited above the electrodes, and it is the part reacting with the targeted VOC. At the end of the metallic paths, large metallic pads are deposited; their role is to make the connection easier between the sensor and the probe station used for the characterization runs detailed in Part III.

The active region of the sensor is located at the center of the device between the two electrodes. These two electrodes end together with an interdigitated-fingers structure presented in Figure 7.

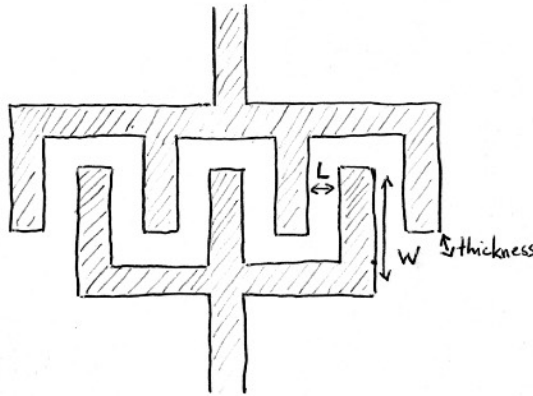


Figure 7 : Interdigitated fingers structure

The approximate resistivity of such a structure is given by (9).

$$R = \rho \frac{L}{A} = \rho \frac{L}{W \times n \text{ of Fingers} \times \text{thickness}} \quad (9)$$

The interdigitated structure increases the contact area between the electrodes and the metal oxide layer. From equation (9) the higher area A reduces the overall film resistance to a range which can be easily monitored by standard instrumentation. With such a structure the overall resistance measured is on the order of 50k Ω . The fabrication process of these interdigitating fingers is presented in the following part.

2. Electrodes Fabrication

The electrodes of the MOS gas sensor are made of platinum. Platinum is a noble metal which produces durable electrodes that avoid any contamination between the electrodes and the metal oxide layer. Since platinum does not adhere well to silicon oxide, a thin layer of Chromium is added between the silicon oxide and platinum. The fabrication of these electrodes is presented as follows.

The first step consists in getting a 12-inch silicon wafer with a 1 μ m silicon oxide layer on top of it. This wafer is cleaned using plasma etching. After the introduction of the wafer into the plasma chamber, the chamber is evacuated to a pressure on the order of 300 mTorr. The chamber is filled with oxygen. Then an alternating voltage is applied between the anode and the cathode of the chamber. This alternating voltage turns oxygen gas into oxygen plasma rich in oxygen ions. These oxygen ions react with organic dust and remove them from the surface of the wafer. This alternating voltage is applied for 30 seconds and then the chamber is refilled with Nitrogen to return to atmospheric pressure. Note that the cleaning step must be done each time the process is stopped. For a pause of few days, a 1 sec plasma etching is enough.

The electrodes are drawn on the wafer using an e-beam lithography process.

The lithography starts with the deposition of the photoresist on the wafer. To enhance the adhesion of the photoresist with the surface of the wafer, a first layer of adhesion promoter HMDS is deposited. HMDS is a “silicon polymer” used to make a connection bridge between silicon oxide and the photoresist. HMDS is deposited by vapor deposition. Multiple vacuum cycles help to reach a final vacuum containing fewer impurities. Then high temperature vapor of HMDS is introduced into the chamber to reach the surface of the wafer. Once HMDS is deposited, the chamber is refilled with Nitrogen, and the wafer can be cooled down before going to the next step.

The next step of the lithography is to spin coat the photoresist on the wafer. The photoresist used is KRS-XE developed by IBM. The 12-inch wafer is placed on a spinner, ~7 ml of photoresist is deposited at the center after being filtered by 0.2µm particle-filter fixed at the output of a 10 ml syringe used for the spin coating. The wafer is spun at 1500 rpm for 70 sec. Immediately after the spin coating, the wafer is soft baked at 120C on a hotplate for 60 sec and cooled down on an metallic support.

The IBM clean room possesses an e-beam lithography system which allows patterning to be implemented without use of a mask. During this step, the interdigitated fingers pattern is drawn on the wafer using an e-beam.

The features drawn are then developed by plunging the wafer in an TMAH bath. KRS-XE resist is a positive photoresist which means that e-beams make the photoresist more soluble. During the development the photoresist is removed where the e-beam has impinged.

Once the pattern of the electrodes are drawn through the photoresist, the metal can be deposited. E-beam evaporation is used to deposit the metals. After the wafer is loaded in the chamber is evacuated to 5 µTorr. To reach this low pressure, two pumps are used, one coarse and one more precise. They are used one after the other and are separated by a crossover step. Once the vacuum is reached, metal can be deposited. Five nm of chromium is deposited, followed by 70 nm of platinum. The metals are heated by an e-beam and because of the high mean free path under such low pressure, metals atoms can evaporate and reach the surface of the wafer. The chamber is then vented and the wafer is retrieved.

The final step, called lift-off, corresponds to the removal of resist and unwanted deposited metal. The wafer needs to go through three different baths.

The first bath is a 57 C NMP N-méthyl-2-pyrrolidone bath for 10 min, which removes most of the metals. It can be observed that the lift begins at the edges of the wafer and around the patterns.

The second bath is a 22 C NMP bath which removes the last part of unwanted metal for 5 minutes. To speed up the removal, ultrasound can be used. However this feature must be used with caution to avoid re-deposition of the metal.

The third bath is a Propanol bath. Propanol is a solvent for NMP and removes NMP from the surface of the wafer. This bath is short and lasts 15 seconds.

To clean the wafer and remove the propanol, the wafer is washed with de-ionized water in a dedicated washer.

Once the deposition of the electrodes is finished, the presence of any defects, dust and conductive bridges between the electrodes is checked under microscope.

3. MOS Layer Deposition

The metal oxide 100 nm layer, which represents the reactive part above the electrodes, can be synthesized using different techniques. Literature shows that such metal oxide layers are deposited mainly by spray, sputtering or sol-gel. The IBM cognitive nose team focuses on sol-gel technique, a well established technology, and a much more recent technology Delayed Ignition of Autocatalytic Combustion Precursors DICO , which is still in development. Even though, these two technologies are not the subject of this thesis, they are briefly presented in the following paragraphs.

Before the deposition of the metal oxide, the sample must undergo some preparation. Indeed previous measurements showed that it can be possible for unwanted metal oxide to be deposited on the side and the bottom of the sample which can lead to electrical shorts when the samples are tested. As a consequence, it is important to guarantee the metal oxide is deposited only on a localized surface. Kapton tape® has been used to restrict the area of metal oxide deposition. A example of sample protection is presented in Figure 8. In this picture, tapes has been placed at the border of the sample. As a consequence, the deposition surface corresponds to the center of the sample. At the end of the electrodes, paper strips have been interleaved between the wafer and the tape in order to prevent adhesive from the tape from remaining on the electrodes.

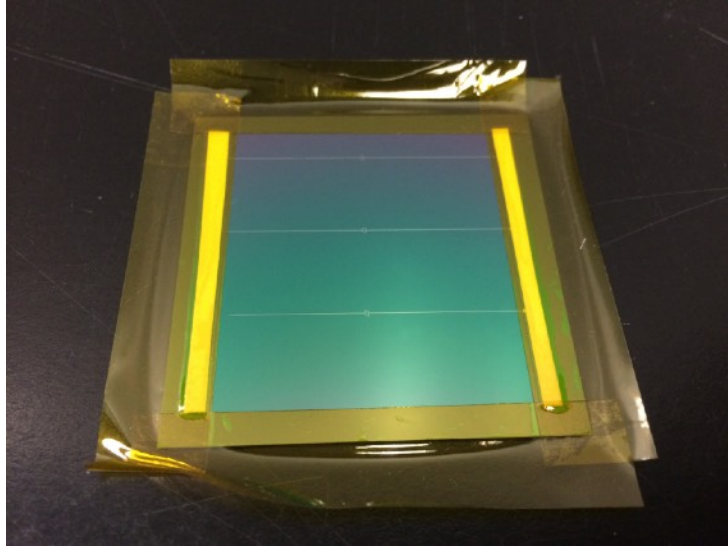


Figure 8 : Use of Kapton® tape to avoid excess of metal oxide

Once the sample is protected, the metal oxide is synthesized either by sol-gel or DICO, presented as follows.

The **sol-gel** process starts from a colloidal solution of precursors — metal alkoxides in this case — in a solvent. By hydrolysis and polycondensation reactions, this solution turns into a gel — a liquid dispersed inside a solid phase. This step is also called aging and lasts multiple hours. The gel is spun on the wafer and then densified by a thermal treatment on a hotplate. Different length of aging may give metal oxide layer with different properties such as porosity and grain size [8].

The **DICO** process starts from a solution containing ionic oxidizers and organic ignition fuels [9]. After the solution is spun on the wafer, the wafer is baked at relatively low temperature of 200C. Combustion initiates and a production of vapors above the wafer can be noticed. DICO appears to be more flexible and controllable than sol-gel. In contrast to sol-gel, for DICO there is no aging reaction, and as a consequence the initial solution can be prepared in advance and used when necessary.

Once the metal layer has been deposited on the interdigitated electrodes, the tapes used to protect the borders of the sample are removed. The connection pads can be deposited.

4. Contact Pads Deposition

When the gas sensor is tested, the device is connected to the characterization set up with needles. A microscope can be used to align the connections, but this step can be time-consuming since the lens must be moved above each pad. To make the connection easier and avoid needing a microscope, one method is to use macroscopic pads. Using e-beam lithography to draw such large pads would be too time-consuming. These pads can be deposited after the fabrication of the electrodes and the deposition of the metal oxide. Since

the positioning of these pads does not require high precision, a photoresist mask can be avoided and replaced by a steel stencil like shown in Figure 9.

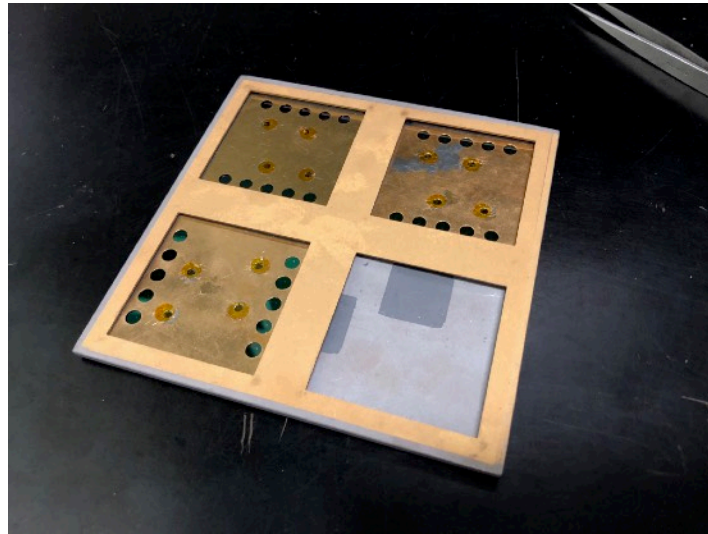


Figure 9 : Steel stencil is used as a mask for the contact pads deposition

The metals are deposited by thermal evaporation. In thermal evaporation, the source material is hosted in a tungsten crucible which is heated by an electrical current using the Joule effect. A typical value of current is 150 A and voltage is 2V. Like the e-beam evaporation used for the electrode deposition, the chamber needs to be in vacuum . Once the pressure inside the chamber reaches $6 \times 10^{-6} Torr$, the evaporation of the metals can start. The first 5 nm layer is made of chromium, used as an adhesion layer. The 100 nm layer is made of a noble metal such as gold or platinum, to avoid pad oxidation. Once the deposition is finished, the chamber is returned to atmospheric pressure and the samples are retrieved. Between runs, the chamber is returned to vacuum to avoid any contamination from room air. Each sample contains 5 devices. The devices are separated by cleaving the sample using a diamond-tipped stylus. Once separated, the devices can proceed to the characterization step.

III.Sensor Characterization And Work Organization

The main goal of this master thesis is the sensors characterization and analysis of their current response. This third part presents the global completion of the project, the set up of the characterization system with the improvements implemented, and the results obtained for a specific study. The study involved here is the search of an optimized solvent for the metal oxide synthesis methods presented in Part II.3.

1. Work Organization

The master thesis described in this report is a 6 month project from March 2018 to August 2018 included. The Gantt Diagram of the project is presented in Figure 10.

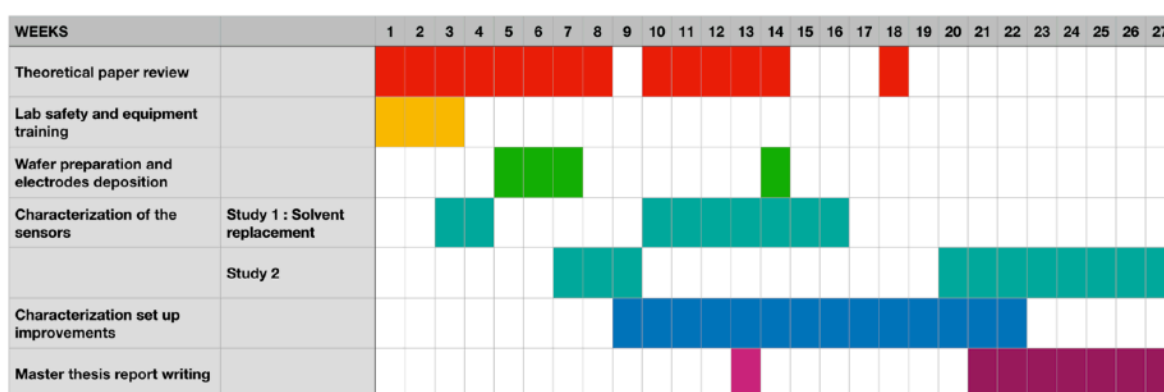


Figure 10 : Gantt diagram of the master thesis

During the first three weeks, a safety and equipment training was completed in order to have access to the IBM Almaden lab facilities and to gain in autonomy. During the first half of the project, a literature review was completed to understand the working principle of the MOS gas sensors, their limitations and their improvement trends. The practical work included preparing the wafers and depositing the test-structures onto the wafers. The wafers were then given to the materials team for metal oxide deposition. After the deposition of the metal oxide the sensor samples were returned in order to be characterized.

Two characterization studies have been made. Both deal with the search for an optimal process for the metal oxide synthesis. The result of the solvent replacement study is presented in Part III.3. In addition, the characterization system has been improved and adapted for the use of other teams. The other teams were working on gas sensors based on other metal oxide deposition techniques or based on polymers and gold nanoparticles.

In order to present the characterization results and define the organization of the tasks, the characterization team and the material team met weekly. In addition, the work done was summarized and sent to the IBM supervisor of the project weekly.

2. Characterization Set Up

The characterization of gas sensors is challenging. Indeed, it requires in parallel the application of a voltage, the measurement of a current, and the delivery of an analyte at a precise concentration and constant flow. Analyte means in this case the gas which needs to be detected by the sensor. For the study of the MOS technology the sensor needs to be heated up to a range of temperature between 200C and 400C. This forces the use of specific materials like steel which must be machined to hold the sensors under-test.

The global schematic of the characterization set up is presented in Figure 11.

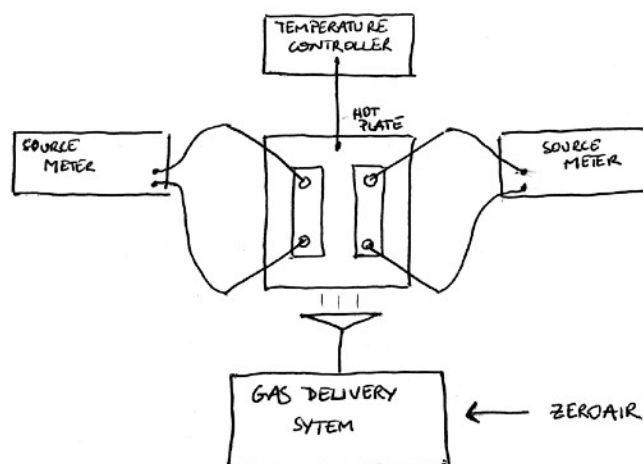


Figure 11 : Global schematic of the MOS gas sensor characterization set up

The probe station can test two sensors at a time. The samples are put on a hot plate and fixed by two steel needles pressed onto the contact pads. The temperature of the hot plate is controlled by a temperature controller. The samples are electrically connected to the SourceMeters by the needles. The references of the two SourceMeters are Keithley 2400 and Keithley 6430. The samples are covered by a metallic cap with a hole from which the gas under test is delivered as shown in Figure 12. The flow gas which contains the target analyte is generated by a gas delivery system. The gas delivery system is presented in detail in Part III.3.

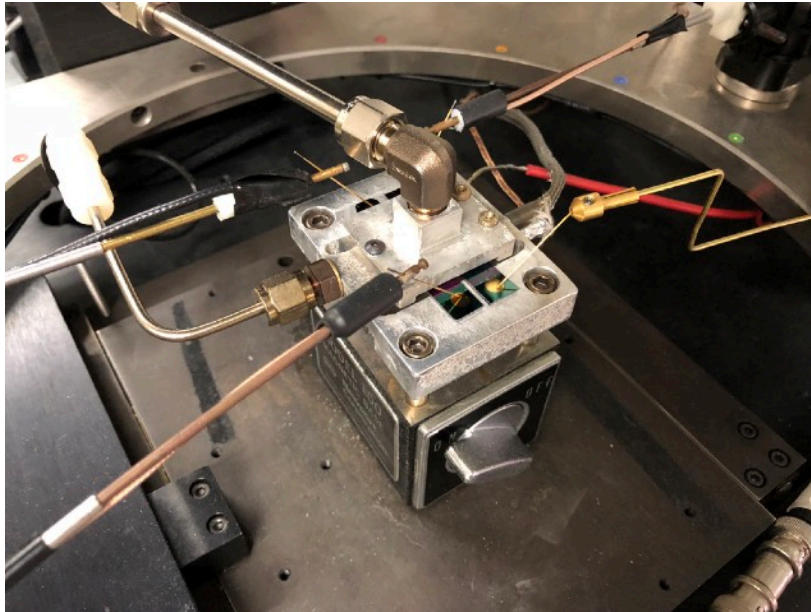


Figure 12 : Probe station holding two gas sensors

As presented in Part I.3, the typical test consists in measuring the evolution of the current while applying a constant voltage of 100 mV, applying, removing or changing concentration of the analyte, and changing the temperature. This means that the test conditions evolve during the test according to a precise chronology. For example, valves need to be closed or opened in a particular order during the test. These modifications can be made manually, but this appears to be time-consuming for the operator and can be a source of possible errors. An application running on a computer controlling the entire system makes the test more consistent from one pair of sensors to another and allows the operator to run the characterization experiments overnight. The different instruments can be controlled by standard protocols via the use of Python scripts with appropriate libraries.

Mass flow controllers (MFCs), valves, and the temperature controller can be connected and controlled by a computer using an RS485-USB interface and serial protocol.

The sourcemeter can be connected and controlled by a computer using GPIB/IEEE488—USB interface and VISA protocol.

The development of the program used for the study presented in this part was initiated by Bastien Delaly and Andrea Fasoli. Multiple corrections and additions to the code have been made by the author to create the final program.

3. Gas Delivery System

The gas delivery represents a key component for the characterization set up and has been fully customized for this purpose. The global gas delivery system is shown in Figure 13. The system is comprised of multiple ovens, MFCs and mixing chambers and is supplied by dry

air coming from IBM Almaden building facilities. The dry air is turned into zero air by a dedicated zero air generator. Zero air is dry air from which rare gases have been removed, so zero air is composed by 25% oxygen O_2 and 75% Nitrogen N_2 . For the sake of simplicity, the gas delivery system containing one oven only is represented in the Figure 14.

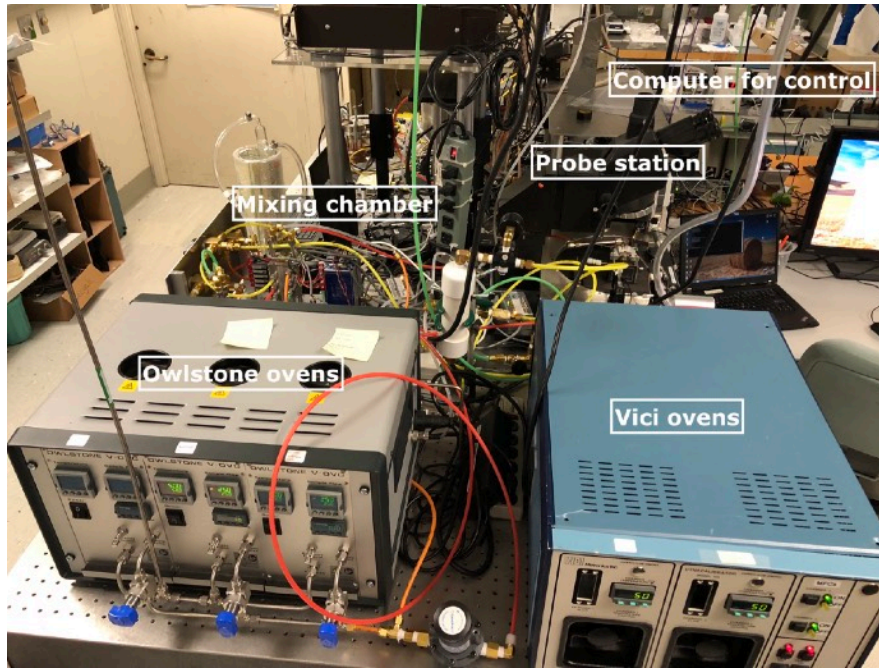


Figure 13 : Picture of the entire gas delivery system

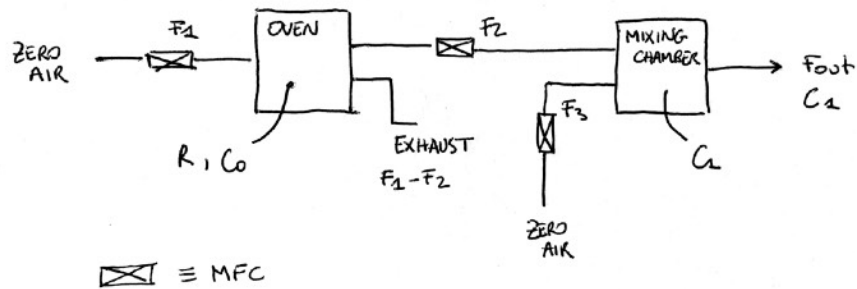


Figure 14: Simplified schematic for gas delivery considering one oven

The ovens used comes from the VICI and Owlstone companies. The oven extracts VOC from a liquid source in a permeation tube by heating it up to a range of temperature between 40C and 100C. An example of permeation tube is presented in Figure 15.



Figure 15 : VOC liquid source inside permeation tube

In addition to the oven, the system includes three mass flow controllers (MFCs) and one mixing chamber. The VOC is generated in the oven at a molar rate $R_m [\frac{mol}{min}]$. The VOC is diluted to reach a low concentration around 100 ppb. The VOC is diluted by adding zero air. The zero air supply has two functions : to dilute and to carry the VOC in the delivery system until reaching the sample. The VOC is diluted a first time in the oven at a concentration C_0 and a second time C_1 in the mixing chamber. The concentrations C_0 and C_1 and the total flow F_{out} are set by the different flows F_1 , F_2 and F_3 tuned by the different MFCs. The expressions of C_0 , C_1 and F_{out} are given respectively by equation (10), equation (11) and equation (12).

$$C_0 = R_m \times \frac{1000}{F_1 + F_2} \quad (10)$$

$$C_1 = C_0 \times \frac{F_2}{F_2 + F_3} \quad (11)$$

$$F_{out} = F_2 + F_3 \quad (12)$$

With the concentration unit $[C] = \frac{mol}{L}$, flow unit $[F] = sccm = \frac{cm^3}{min}$ and molar rate unit $[R_m] = \frac{mol}{min}$.

The rate of analyte delivery from the oven is calculated experimentally by monitoring the loss of weight of the permeation source. Figure 16 presents the evolution of the permeation source weight over time.

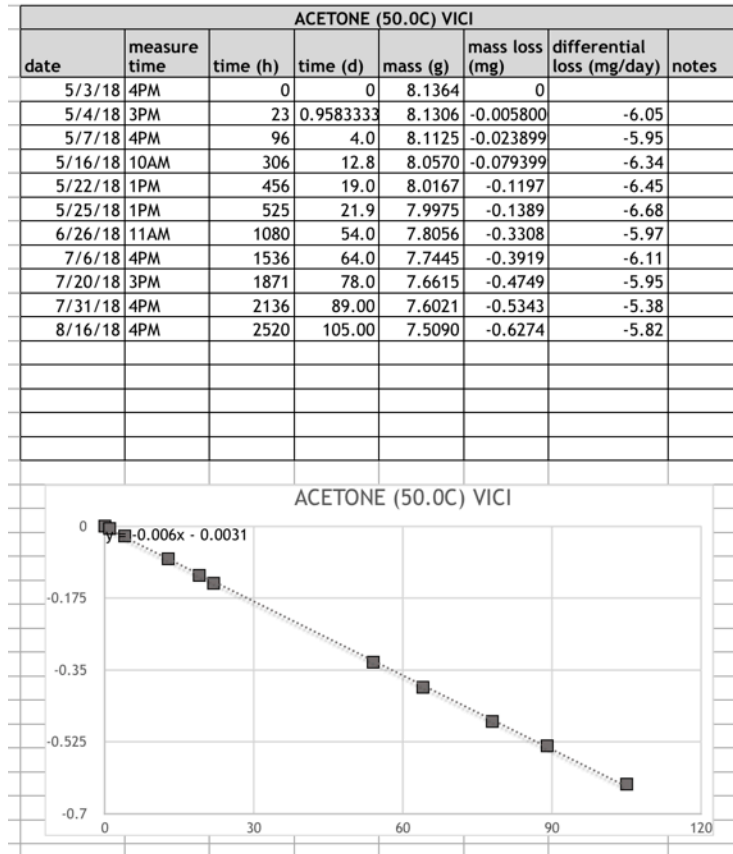


Figure 16 : Weight monitoring of the permeation source

The rate R of analyte delivery is deduced from the linear extrapolation of the weight loss curve obtained. The molar rate R_m is calculated using the molar mass of the analyte $M_{analyte}$ and equation (13).

$$R_m = \frac{R}{M_{analyte}} \quad (13)$$

With molar rate unit $[R_m] = \frac{mol}{min}$, rate unit $[R] = \frac{mg}{min}$ and molar mass $[M] = \frac{mg}{mol}$.

Typical values used for the characterization under acetone exposure are :

$$NA : \begin{cases} T_{oven} = 50 \text{ C} \\ R = 5.8 \text{ mg/day} \\ M_{acetone} = 58.08 \text{ g/mol} \\ F_1 = 100 \text{ sccm} \\ F_2 = 7.2 \text{ sccm} \\ F_3 = 500 \text{ sccm} \\ C_1 = 205 \text{ ppb} \\ F_{out} \approx 500 \text{ sccm} \end{cases}$$

In this configuration, the sensitivity of the sensor is measure for acetone at 200 ppb. By tuning F_1 between 30 and 2000 sccm and F_2 between 1 and 20 sccm (corresponding to the operating limits of the MFCs) and keeping F_3 at 500 sccm, the concentration of acetone can vary from 0.5 ppb and 500 ppb. If an higher concentration is required, one solution can be a higher temperature in the oven to increase the permeation rate. Note that the rate must be re-computed experimentally if the temperature of the oven is changed.

4. Solvent Replacement Study And Interpretation

Objectives

The solvent commonly used for the metal oxide synthesis — 2methoxyethanol — is reported to be harmful for the operator [15]. Being part of the MOS team of the cognitive nose project, the author focused on fabricating sensors using safer alternative solvents for sol-gel and DICO processes presented in Part II.3. This study evaluates the sensors produced with candidate new solvents to determine their sensitivity to acetone. These solvents were chosen for their proximity with 2methoxyethanol according to their polarity, Hansen solubility parameters, and boiling point. The results were presented to the MOS team for use in evaluating the candidate new solvents.

The samples studied were divided in four categories depending on the type of process sol-gel or DICO and the metal Tin or Indium. Since the optimal operating temperature was not known, the performance of the sensors needed to be evaluate at different temperatures for better comparison between the sensors. To make the comparison relevant, the MOS team made sure to produce sensors with metal oxide thicknesses around 70 nm. By automating the characterization system, it was feasible for the author to evaluate several samples for one process and get results which more statistics.

Protocol

The samples were characterized according to the following protocol. The samples were annealed during 6 hours at 300 C under 2000 sccm of dry air. This preliminary step is required to dry the samples and remove the compounds absorbed by the metal oxide layer. For the testing procedure, the samples underwent a cycle with a constant flow at 500 sccm for each temperature considered — 400 C to 240 C with a 20 C step in between. For one cycle, the samples received dry air for 100 seconds, then acetone at concentration of 200 ppb for 10 minutes, and finally dry air for up to 60 minutes waiting for recovery. Cycles were separated by period of 30 minutes with dry air at 500 sccm to wait for the temperature and the current response to stabilize. The protocol used is summarized in Table 2.

	Period	F_1 [sccm]	F_2 [sccm]	F_3 [sccm]	V [mV]	T [C]	F_{out} [sccm]	C_1 [ppb]
Annealing	6 h	100	0	2000	100	300	2000	0
Stabilization	30 min	100	0	500	100	400	500	0
Sensing	100 sec	100	0	500	100	400	500	0
	10 min	100	7.2	500	100	400	500	200
	60 min	100	0	500	100	400	500	0
Stabilization	30 min	100	0	500	100	380	500	0
Sensing	100 sec	100	0	500	100	380	500	0
	10 min	100	7.2	500	100	380	500	200
	60 min	100	0	500	100	380	500	0
Stabilization	30 min	100	0	500	100	380	500	0
...
Stabilization	30 min	100	0	500	100	240	500	0
Sensing	100 sec	100	0	500	100	240	500	0
	10 min	100	7.2	500	100	240	500	200
	60 min	100	0	500	100	240	500	0

Table 2 : Characterization protocol

Results

- **Characterization of one particular process, one metal oxide and one solvent.**

Figure 17 presents the characterization results under 200 ppb acetone obtained for SnO₂ obtained by DICO using 2-methoxyethanol as solvent. These results consist in the evolution of the current response through the sensor for a working temperature going from 360 C to 240 C. Three periods can be distinguished, the first one between 0 and 100 seconds which corresponds to the initial zero air period, the second one between 100 and 700 seconds which corresponds to the exposure to acetone and the third period after 700 seconds which correspond to the recovery dry air period. Table 3 shows the precise parameters defined in Part I.3 obtained from the curves. In particular it shows that the current jumps by several μ A between the zero air period and the exposure period. Looking at the sensitivity column, it appears that the sensitivity is maximized at temperature of 280 C. These results are in agreement with the literature review presented in Part I.

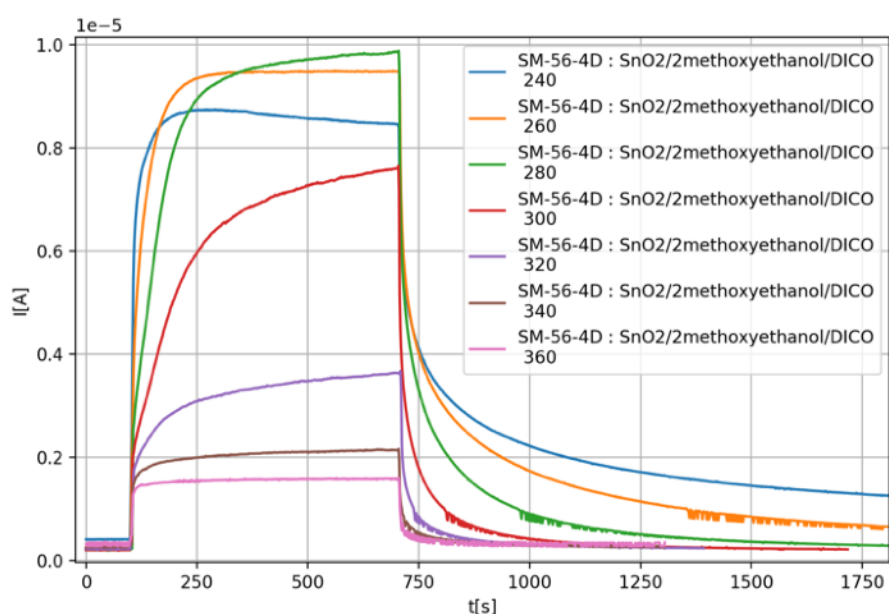


Figure 17 : Current response under 200 ppb acetone for SnO2 produced by DICO using 2methoxyethanol

T [C]	Base current [uA]	Max current [uA]	Sensitivity	Response time [s]	Recovery time [s]
240	0.4	8.61	21.2	37	1326
260	0.24	9.47	39	72	735
280	0.2	9.64	47.7	147	429
300	0.2	7.09	35.3	287	312
320	0.22	3.41	15.5	276	281
340	0.26	2.09	7.9	121	259
360	0.3	1.57	5	39	227

Table 3 : Extracted data from the current response of SnO2 DICO 2methoxyethanol

- **Characterization of one particular process, one particular metal oxide with different solvents.**

Figure 18 shows the evolution of the different current response parameters under 200 ppb acetone across a range of temperature between 400 C and 240 C for SnO2 obtained by DICO using different solvents : 2methoxyethanol, ethyl-lactate, 1 propanol and PMOH. For one solvent, multiple characterizations have been made to guarantee the reliability of the results.

It should be pointed that the optimal temperature — for which the maximum of sensitivity is obtained — does not depend on the solvent and is around 280 C. At the peak of sensitivity, the base current reaches a minimum and the maximal current a maximum. Looking at the different sensitivity curves, sensors produced using ethyl-lactate and PMOH present a sensitivity 10% higher than the ones produced with 2-methoxyethanol. As a consequence, ethyl-lactate and PMOH appear to be promising 2-methoxyethanol replacements.

Considering the recovery time plot, the recovery time increases when the temperature decreases. This is in correlation with the deceleration of a chemical reaction when the temperature is decreased. More precisely, the recovery time is multiplied by 3 from the optimal temperature 280C to 240 C. At the optimal temperature the recovery time is at 3 min which is not negligible.

Focusing on the response time, it is remarkable that the response time does not follow the same trend as the recovery time. Indeed, the response time presents a peak at a temperature slightly higher than the temperature for optimal sensitivity. This peak of sensitivity is linked to a change in current response shape as shown in Figure 19. This may be explained by a change in the species population on the metal oxide surface. Table 1 shows that hydroxide groups -OH are completely removed after 400 C which means that starting from 300 C the hydroxide groups begin to leave the surface.

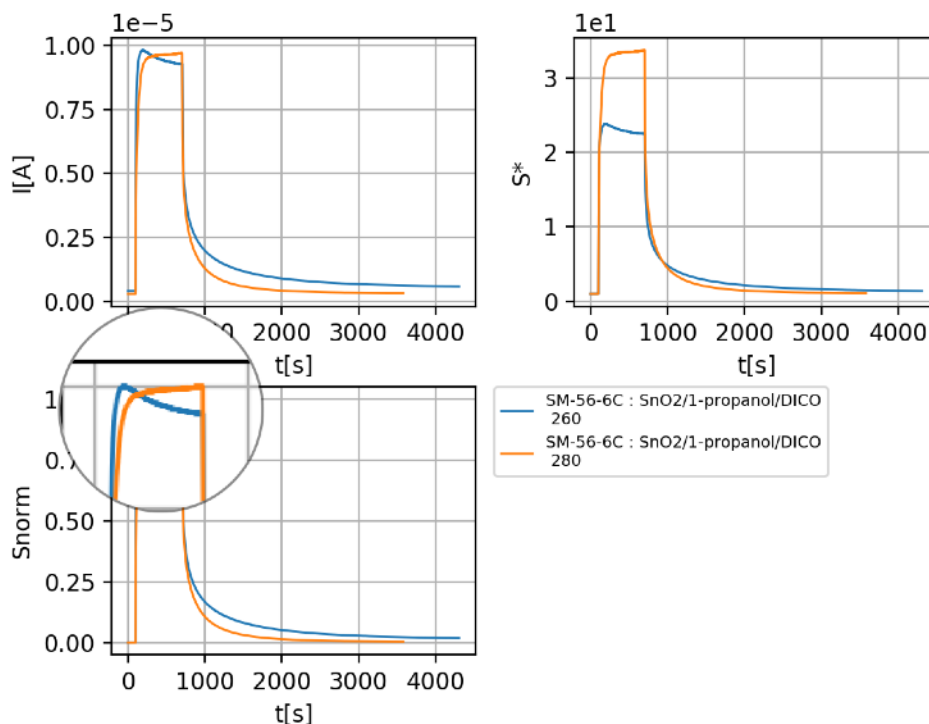


Figure 19 : Change of current response shape

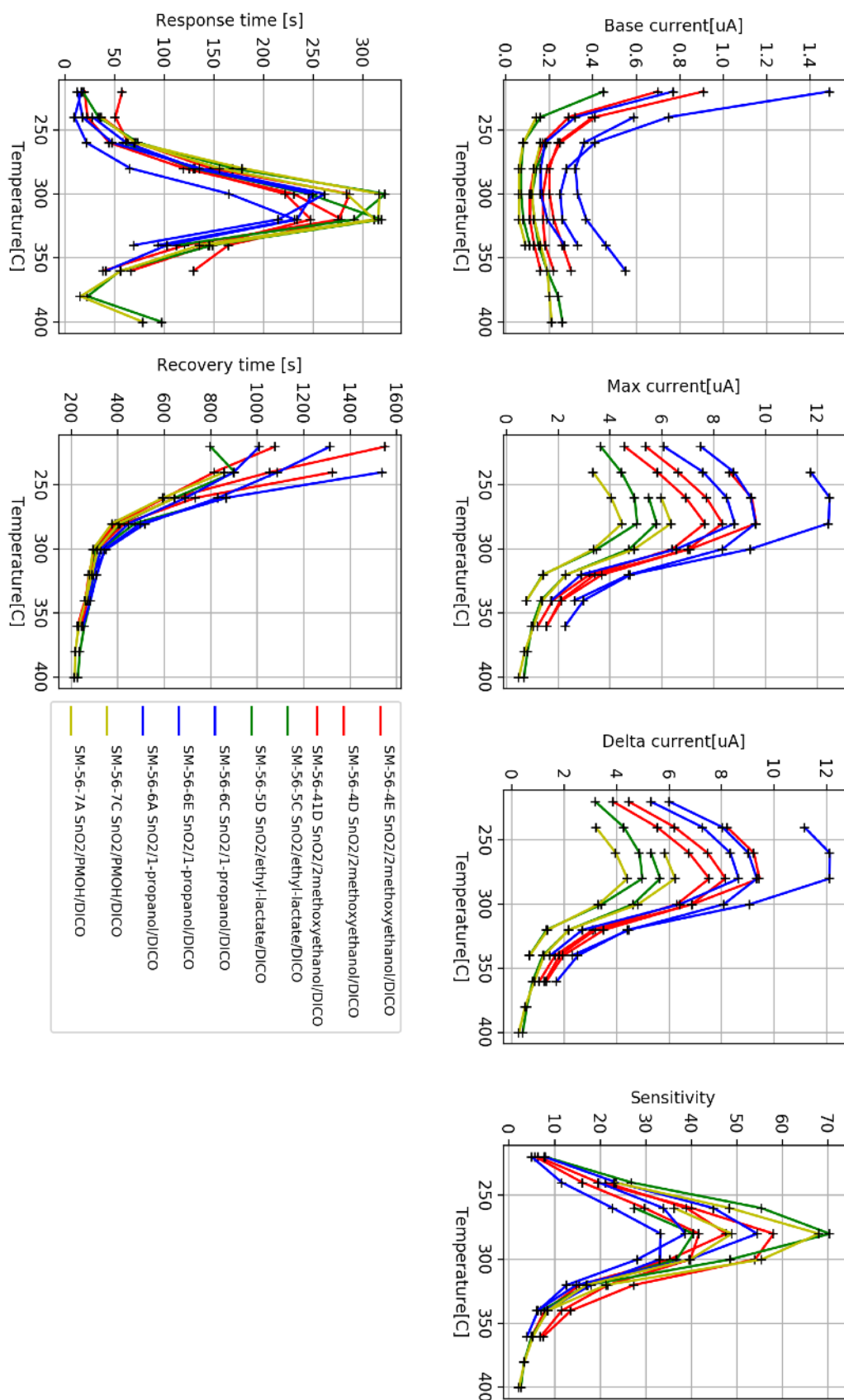


Figure 18 : Evolution of performance under 200 ppb acetone of SnO₂ DICO with different solvents according to the temperature

- **Characterization of different processes with different metal oxide with different solvents.**

Table 4 summarizes the performance under 200 ppb acetone at the optimal temperature for SnO₂ and In₂O₃ produced by DICO and sol-gel using different solvents : 2-methoxyethanol, ethyl-lactate, 1-propanol, PMOH and 2-methyl-1-butanol.

For each pair of metal oxide processes, DICO or sol-gel, the optimal temperature does not depend on the solvent used.

SnO₂ presents up to 5 times higher sensitivity than In₂O₃. SnO₂ is therefore a better choice to sense acetone than In₂O₃.

Regardless of the solvent used, DICO presents sensitivity 10 to 20 % higher than sol-gel. Since DICO has a more robust process than sol-gel, DICO appears to be a preferable process to produce the metal oxide layer of the MOS sensors.

For each pair of metal oxide processes, DICO or sol-gel, the sensitivity obtained with 2-methoxyethanol is compared with other solvents. In each case, solvent replacements exist and present similar if not higher sensitivity.

For the sensors which present the highest sensitivity, it should be considered that the response time reaches 3 minutes and recovery time reaches 7 minutes which is again not negligible.

Process	Metal	Solvent	T optimal [C]	Sensitivity	Response time [s]	Recovery time [s]
DICO	SnO ₂	2methoxyethanol	280	50±10	150	430
		ethyl-lactate	280	55±15	150	430
		1-propanol	280	40±10	150	450
		PMOH	280	60±10	150	430
	In ₂ O ₃	2methoxyethanol	320	11±2	50	300
		ethyl-lactate	320	7±2	30	300
		PMOH	320	10±1	50	300
Sol-gel	In ₂ O ₃	ethyl-lactate	380	5	30	300
	SnO ₂	2methoxyethanol	260	45±3	250	500
		n-Butanol	260	43±2	250	500
		1-propanol	260	32±5	250	500
		2-methyl-1-butanol	260	37±2	200	500

Table 4 : Summary of performance under 200 ppb acetone for SnO₂ and In₂O₃ produced by DICO and sol gel with different solvents

5. Improvement Of The Characterization Set Up For Next Study

The characterization set up presented in this report has some limitations.

The open chamber is the first limitation. With an open chamber, the air from the environment can pollute the measurements. As a consequence, a relatively high flow on the sensor is required to guarantee that the sensor is in contact only with the flow generated by the oven. Also, an open chamber precludes the use of any harmful gas, for the safety of the operator, which limits, the range of the study. To overcome these difficulties, the electronic nose team plans to design a closed chamber.

The second limitation of the present characterization set up is the number of sensor under test. The evaluation of the recipes requires as many sensor characterizations as possible. Having a automated script helps to get a higher amount of data; characterizing a higher number of samples per run will provides a better picture of the performance of the sensors. The author developed another acquisition system capable of testing 8 sensors in parallel. This new system relies on the use of an Keithley Switch which makes the connections between the sensors under test and the source meter one after the other. This system is monitored by a Python script presented in Appendix 1. This new system is already used by the Polymer sensor team and will be implemented for the MOS characterization set up.

Conclusion

This thesis presents MOS gas sensors' working principle, possible fabrication processes, and proposes an automated characterization set up to evaluate the performance of the gas sensors. MOS gas sensors are based on a resistivity change in presence of VOC. The sensitivity and reactivity of gas sensors depend on different parameters starting from the design of the architecture to the synthesis of the metal oxide. Identifying the best sensor requires reliable test results which needs a robust characterization set up. Specific equipments controlled by computer via standard protocols are the keys creating a reliable characterization set up. Using the proposed characterization set up, the author was able to quantify the performance of gas sensors produced by different processes, in a consistent manner that allows the results to easily compared across fabrication processes. From this study, it appears that DICO process — a recent process that is comparatively easier to implement— shows higher sensitivity than sol-gel. This study also tells that 2-methoxyethanol — a solvent commonly used for the synthesis of metal oxide layers, but which may be harmful for the operator — can be replaced by other solvents. This thesis proposes possible future studies and systems improvement for the characterization set up. The investigation on the different oxidizers used for DICO process may lead to interesting results. The characterization set up can be improved by the implementation of a closed chamber and the implementation of a scan system to measure several samples simultaneously.

Appendix

Appendix 1 : Multiple sensors characterization script

polymerChamberScript.py
Saved: 7/9/18, 3:00:03 PM

Page 1/2
Printed for: Antoine PISSIS

```
1 """
2 Created on Wed May 30 12:00:00 2018
3 @author: Antoine Pissis
4 """
5
6 """
7 Automation of the I(t) measurement of the 8 samples inside the polymer chamber following the protocol
8 described in polymerChamberScriptProtocol.txt . Gases flow generated by Owlstone ovens and tuned by MFC.
9 Current measurement done by Keitley source meter and sample selection done using Keitley switch.
10 """
11
12 ## LIBRARIES
13 import numpy #math library
14 import matplotlib.pyplot as plt #plot library
15 import matplotlib.animation as animation #plot animation
16 import visa #instrument connection library
17 import serial #instrument connection library
18 import time #time library
19
20 ## VARIABLES
21
22 # Connection strings for Source Meter and Switch using VISA
23 sourceMeterConnectionString = 'GPIB0::16::INSTR'
24 switchConnectionString = 'GPIB0::7::INSTR'
25
26 # Connection strings for MFC and mixing chamber valves using SERIAL
27 lineSerialPort = 'COM4'
28
29 # Protocol file containing the schedule of the Flows [sccm]
30 protocolFile = 'protocol1.txt'
31
32 # Voltage bias [V]
33 voltageBias = 1
34
35 # Scan rate [s]
36 waitTime = 0.1
37
38 # Number of set and sample
39 nbSets = 2
40 nbSamplesPerSet = 4
41 nbSamples = nbSets * nbSamplesPerSet
42
43 ## FUNCTIONS
44
45 def establishConnectionVisa(connectionString) :
46     """
47     Establish connection to the instrument which is identified by connectionString using VISA protocol.
48     Return the handle of the instrument for further communication.
49     """
50     rm = visa.ResourceManager()
51     try :
52         handle = rm.open_resource(connectionString) # create handle and open connection
53         print('Connected to ' + connectionString)
54     except :
55         print('Failed connection to : ' + connectionString)
56     return handle # return handle
57
58 def establishConnectionSerial(serialPort) :
59     """
60     Establish the connection with the serial line identified by serialPort using SERIAL protocol.
61     Return the serial.
62     """
63     ser = serial.Serial() # create serial
64     ser.port = serialPort # associate the serial and port
65     try :
66         ser.open()
67         print('Connected on port', ser.port)
68     except :
69         print('Failed to connect to port', ser.port)
70     return ser
71
72 def updatePlots(fig,AX,T,I) :
73     """
74     Update plot inside fig and AX according to the new values of T and I.
75     """
76     for i in range(nbSets) :
77         for j in range(nbSamplesPerSet) :
78             AX[i][j].set_ylabel('Current [A]')
79             AX[i][j].set_xlabel('Time [s]')
80             AX[i][j].set_title('Sample '+str(i*nbSamplesPerSet+j+1))
81             AX[i][j].plot(T[i*nbSamplesPerSet+j],I[i*nbSamplesPerSet+j], 'bs ',markeredgecolor='b',linestyle="None")
82             AX[i][j].autoscale()
83     fig.canvas.flush_events()
84
85 def sense(stopTime,t0,fig,AX,T,I,hsw,hsm) :
86     """
87     Launch sensing, collect, plot and save data.
88     """
89     while time.time() - t0 < stopTime : # will loop until sensing time reached
90         for i in range(nbSamples) : # scan each sample one after the other
91             hsw.write(':OPEN ALL') # disable electrical connection
92             hsw.write(':CLOS (@ 1!21, 1!'+str(i+1)+')') # enable electrical connect to the sample
93             time.sleep(waitTime) # wait
94             Itemp = hsm.query('G4,2,0X') # pick current
95             ttemp = time.time()-t0 # pick time
96             (globals()['data_file'+str(i+1)]).write(str(ttemp)+'\t'+Itemp[:2]+'\\n') # save time and current in data file
97             T[i].append(ttemp) # save time for plotting
98             I[i].append(Intemp) # save current for plotting
99     updatePlots(fig,AX,T,I)
100
```

```

101 def setFlows(flowAnalyte,flowDryAir,ser) :
102     """
103     Configure the gases system in order to get the right flows.
104     """
105
106     # Set Dry Air flow
107     print('here')
108     ser.write('@@113SX!' + str(flowDryAir) + ';FF').encode()
109     ser.write('@210N1\r\n'.encode())
110
111     # Set Analyte Flow
112     if flowAnalyte == 0 :
113         ser.write('@210P5\r\n'.encode())
114     else :
115         ser.write('@@113SX!' + str(flowAnalyte) + ';FF').encode()
116         ser.write('@210N5\r\n'.encode())
117
118 def main():
119
120     print('\n ++++++ POLYMER CHAMBER SENSING ++++++ \n')
121
122     # STEP 1 : Establish connections
123     print('STEP 1 : Establish connections')
124
125     hsm = establishConnectionVisa(sourceMeterConnectionString) # create handle source meter
126     hsw = establishConnectionVisa(switchConnectionString) # create handle switch
127     ser = establishConnectionSerial(lineSerialPort) # establish serial connection
128
129     print('Connections established \n')
130
131     # STEP 2 : Initialize source meter
132     print('STEP 2 : Initialize source meter')
133
134     hsm.write('F0,OX') # set source : voltage, measure : current, DC
135     hsm.write('B' + str(voltageBias) + ',0,X') # set voltage bias
136     hsm.write('L500E-6,7X') # set compliance and measure range
137     hsm.write('P2X') # set 4 readings for 1 measurement
138     hsm.write('OOX') # deactivate remote sensing
139     hsm.write('NIX') # operate
140     hsm.write('HOX') # trigger
141
142     print('Source meter initialized \n')
143
144     # STEP 3 : Create data files and set plots
145     print('STEP 3 : Open data files and set plots')
146
147     for i in range(nbSamples) :
148         globals()['data_file'+str(i+1)] = open('./DATA/Data_sample'+str(i+1)+'.txt', 'w')
149
150
151     plt.ion()
152     fig, AX = plt.subplots(nrows=nbSets, ncols=nbSamplesPerSet)
153
154     T = [[] for i in range(nbSamples)]
155     I = [[] for i in range(nbSamples)]
156
157     print('Data files opened and plots set\n')
158
159     # STEP 4 : Sense
160     print('STEP 4 : Sensing ...')
161
162     t0 = time.time() # define time reference
163
164     with open(protocolFile) as f :
165         for line in f.readlines()[1:] :
166             stopTime = int(line.split('\t')[0])
167             flowAnalyte = int(line.split('\t')[1])
168             flowDryAir = int(line.split('\t')[2])
169
170             print(stopTime, flowAnalyte, flowDryAir)
171
172             setFlows(flowAnalyte,flowDryAir,ser)
173             sense(stopTime,t0,fig,AX,T,I,hsw,hsm)
174
175     print('Sensing completed \n')
176
177     # STEP 5 : Close data files
178     print('STEP 5 : Close data files')
179     for i in range(nbSamples) :
180         (globals()['data_file'+str(i+1)]).close()
181
182     print('Data files closed')
183
184     print('\n ++++++ END ++++++')
185
186 if __name__ == '__main__' :
187     main() # call main() function when python is launched
    
```

Bibliography

[1] Yamazoe, Noboru. "Toward Innovations of Gas Sensor Technology." *Sensors and Actuators, B: Chemical* 108, no. 1–2 SPEC. ISS. (2005): 2–14. <https://doi.org/10.1016/j.snb.2004.12.075>.

[2] Schultealbert, Caroline, Tobias Baur, Andreas Schütze, Stefan Böttcher, and Tilman Sauerwald. "A Novel Approach towards Calibrated Measurement of Trace Gases Using Metal Oxide Semiconductor Sensors." *Sensors and Actuators, B: Chemical* 239 (2017): 390–96. <https://doi.org/10.1016/j.snb.2016.08.002>.

[3] Seiyama, T., Kato, A., Fujiishi, K. and Nagatani, M. (1962) A New Detector for Gaseous Components Using Semiconductive Thin Films. *Analytical Chemistry*, 34, 1502-1503. <http://dx.doi.org/10.1021/ac60191a001>

[4] Sakai, Go, Naoki Matsunaga, Kengo Shimano, and Noboru Yamazoe. "Theory of Gas-Diffusion Controlled Sensitivity for Thin [®] Lm Semiconductor Gas Sensor." *Sensors and Actuators B: Chemical* 80 (2001): 125–31. [https://doi.org/10.1016/S0925-4005\(01\)00890-5](https://doi.org/10.1016/S0925-4005(01)00890-5).

[5] Varpula, A., S. Novikov, J. Sinkkonen, and M. Utriainen. "Bias Dependent Sensitivity in Metal-Oxide Gas Sensors." *Sensors and Actuators, B: Chemical* 131, no. 1 (2008): 134–42. <https://doi.org/10.1016/j.snb.2007.12.013>.

[6] Korotcenkov, G., and B. K. Cho. "Thin Film SnO₂-Based Gas Sensors: Film Thickness Influence." *Sensors and Actuators, B: Chemical* 142, no. 1 (2009): 321–30. <https://doi.org/10.1016/j.snb.2009.08.006>.

[7] Yamazoe, N. Et al. "Interactions of tin oxide surface with O₂, H₂O and H₂" *Surface Science* 86 (1979) 335-344 [https://doi.org/10.1016/0039-6028\(79\)90411-4](https://doi.org/10.1016/0039-6028(79)90411-4)

[8] Brinker, C. J., R. Sehgal, S. L. Hietala, R. Deshpande, D. M. Smith, D. Loy, and C. S. Ashley. "Sol-Gel Strategies for Controlled Porosity Inorganic Materials." *Journal of Membrane Science* 94, no. 1 (1994): 85–102. [https://doi.org/10.1016/0376-7388\(93\)E0129-8](https://doi.org/10.1016/0376-7388(93)E0129-8).

[9] Lioni, K, A Fasoli, L Sundberg, Francesco Ceccarelli, R. D Miller, and L. Bozano. "Evaluation of In₂O₃ Prepared by the Delayed Ignition Combustion Process as a Gas Sensor," 2018, 219–22. <https://re.public.polimi.it/handle/11311/1046826#.W2orS5zWRbI.mendeley>.

[10] Korotcenkov, G., and B. K. Cho. "Instability of Metal Oxide-Based Conductometric Gas Sensors and Approaches to Stability Improvement (Short Survey)." *Sensors and Actuators, B: Chemical* 156, no. 2 (2011): 527–38. <https://doi.org/10.1016/j.snb.2011.02.024>.

[11] Ippolito, S J, S Kandasamy, K Kalantar-zadeh, and W Wlodarski. "Hydrogen Sensing Characteristics of WO₃ Thin Film Conductometric Sensors Activated by Pt and Au Catalysts." *Sensors and Actuators B: Chemical* 108, no. 1 (2005): 154–58. <https://doi.org/https://doi.org/10.1016/j.snb.2004.11.092>.

[12] <http://www.maskau.dk/projects/electronic-nose>

[13] Wilson, Alphus Dan. "Review of Electronic-Nose Technologies and Algorithms to Detect Hazardous Chemicals in the Environment." *Procedia Technology* 1 (2012): 453–63. <https://doi.org/10.1016/j.protcy.2012.02.101>.

[14] Nakhleh, Morad K., Haitham Amal, Raneen Jeries, Yoav Y. Broza, Manal Aboud, Alaa Gharra, Hodaya Ivgi, et al. "Diagnosis and Classification of 17 Diseases from 1404 Subjects via Pattern Analysis of Exhaled Molecules." *ACS Nano* 11, no. 1 (2017): 112–25. <https://doi.org/10.1021/acsnano.6b04930>.

[15] <https://www.bloomberg.com/news/features/2017-06-15/american-chipmakers-had-a-toxic-problem-so-they-outsourced-it>

[16] Myung-Gil Kim, Jonathan W. Hennek, Hyun Sung Kim, Mercouri G. Kanatzidis, Antonio Facchetti, and Tobin J. Marks, "Delayed Ignition of Autocatalytic Combustion Precursors: Low-Temperature Nanomaterial Binder Approach to Electronically Functional Oxide Films" *J. Am. Chem. Soc.* 2012, 134, 11583–11593 [dx.doi.org/10.1021/ja301941q](https://doi.org/10.1021/ja301941q)